Multidimensional treatment of stochastic solvent dynamics in photoinduced proton-coupled electron transfer processes: Sequential, concerted, and complex branching mechanisms

ARTICLE *in* THE JOURNAL OF CHEMICAL PHYSICS · OCTOBER 2011

Impact Factor: 2.95 · DOI: 10.1063/1.3651083 · Source: PubMed

3 AUTHORS, INCLUDING:

Alexander V. Soudackov
University of Illinois, Urbana-Champaign
54 PUBLICATIONS **1,753** CITATIONS

SEE PROFILE

Multidimensional treatment of stochastic solvent dynamics in photoinduced proton-coupled electron transfer processes: Sequential, concerted, and complex branching mechanisms

Alexander V. Soudackov, Anirban Hazra, and Sharon Hammes-Schiffer

Citation: J. Chem. Phys. **135**, 144115 (2011); doi: 10.1063/1.3651083
View online: http://dx.doi.org/10.1063/1.3651083
View Table of Contents: http://jcp.aip.org/resource/1/JCPSA6/v135/i14
Published by the American Institute of Physics.

Multidimensional treatment of stochastic solvent dynamics in photoinduced proton-coupled electron transfer processes: Sequential, concerted, and complex branching mechanisms

Alexander V. Soudackov, Anirban Hazra, and Sharon Hammes-Schiffer[a)]
Department of Chemistry, Pennsylvania State University, University Park, Pennsylvania 16802, USA

(Received 25 July 2011; accepted 22 September 2011; published online 13 October 2011)

A theoretical approach for the multidimensional treatment of photoinduced proton-coupled electron transfer (PCET) processes in solution is presented. This methodology is based on the multistate continuum theory with an arbitrary number of diabatic electronic states representing the relevant charge distributions in a general PCET system. The active electrons and transferring proton(s) are treated quantum mechanically, and the electron-proton vibronic free energy surfaces are represented as functions of multiple scalar solvent coordinates corresponding to the single electron and proton transfer reactions involved in the PCET process. A dynamical formulation of the dielectric continuum theory is used to derive a set of coupled generalized Langevin equations of motion describing the time evolution of these collective solvent coordinates. The parameters in the Langevin equations depend on the solvent properties, such as the dielectric constants, relaxation time, and molecular moment of inertia, as well as the solute properties. The dynamics of selected intramolecular nuclear coordinates, such as the proton donor-acceptor distance or a torsional angle within the PCET complex, may also be included in this formulation. A surface hopping method in conjunction with the Langevin equations of motion is used to simulate the nonadiabatic dynamics on the multidimensional electron-proton vibronic free energy surfaces following photoexcitation. This theoretical treatment enables the description of both sequential and concerted mechanisms, as well as more complex processes involving a combination of these mechanisms. The application of this methodology to a series of model systems corresponding to collinear and orthogonal PCET illustrates fundamental aspects of these different mechanisms and elucidates the significance of proton vibrational relaxation and nonequilibrium solvent dynamics. [doi:10.1063/1.3651083]

I. INTRODUCTION

Photoinduced proton-coupled electron transfer (PCET) processes, which involve both electron transfer (ET) and proton transfer (PT), are ubiquitous in chemistry and biology. In particular, photoinduced PCET reactions play an important role in energy conversion devices such as solar cells, artificial and natural photosynthetic systems,[1–8] DNA exposed to radiation,[9,10] and solution-semiconductor interfaces.[11] Understanding the fundamental principles governing these reactions is a key factor in designing new devices and improving existing devices by tuning the physical and chemical characteristics of their components. Recent advances in time-resolved spectroscopic techniques provide new opportunities for directly probing nonequilibrium relaxation processes in PCET systems following photoexcitation.[12]

Various types of photoinduced PCET processes in solution have been studied experimentally with spectroscopic techniques. In one type of system, the PCET process is instigated by excitation to a metal-to-ligand charge transfer (MLCT) state in a transition metal complex. In this case, the relaxation dynamics involves the quenching of the MLCT state by electron transfer from a donor molecule to the transition metal in conjunction with a proton transfer reaction usually involving the donor molecule. Typical examples of such systems include photosystem II and biomimetic models containing Ru complexes.[12–15] In another type of system, the PCET process is instigated by intramolecular electron transfer within a conjugated molecule that is hydrogen bonded to a base. In this case, the relaxation dynamics involves intramolecular ET in conjunction with proton transfer to the base. An example of such a system is the hydrogen-bonded adduct of p-nitrophenylphenol and tert-butylamine.[16,17] In all of these systems, the PCET mechanism could be sequential (ET-PT or PT-ET), concerted (EPT), or a combination of sequential and concerted pathways.

An important feature of these processes is that the charge distributions in the ground state prior to optical excitation are substantially different from those in the photoexcited, charge-separated state. This feature leads to a highly nonequilibrium configuration of the solvent immediately following photoexcitation. In addition, the proton potential in the photoexcited state could differ from that in the ground state, leading to the population of excited proton vibrational states according to the Franck-Condon principle. As a result, photoinduced PCET processes may be coupled to solvent and proton vibrational relaxation dynamics that significantly impact the overall mechanism and relaxation timescale. The development of theoretical approaches that describe these dynamical effects

a)Author to whom correspondence should be addressed. Electronic mail: shs@chem.psu.edu.

is critical for the accurate modeling of experimentally studied photoinduced PCET processes.

The importance of solvent dynamical effects for ET reactions in solution has been recognized and discussed extensively in the literature.[18–27] The majority of theoretical models for PCET reactions,[28–30] however, have neglected solvent dynamical effects, assuming that the solvent remains in equilibrium during the reaction. Early efforts to include solvent dynamics explicitly[31,32] were based on simple phenomenological models that were difficult to relate to experimental systems. More recently, we studied photoinduced PCET reactions using a model Hamiltonian based on a two-state system coupled to a harmonic bath and derived the equations of motion for the reduced density matrix elements in an electron-proton vibronic basis.[33,34] The main advantage of this approach is that the quantum coherence may be included in the analysis by propagating the off-diagonal elements of the reduced density matrix. The disadvantages of this approach are that it is restricted to a specific coupling regime and relies on the assumption that the solvent remains in equilibrium throughout the electron-proton transfer process. The latter assumption is valid for photoinduced reactions in which the timescale of the solvent dynamics is much faster than the timescale of the electron-proton transfer process but breaks down when the solvent dynamics and electron-proton transfer occur on similar timescales.

To investigate the nonequilibrium solvent dynamics in these processes, we developed a theoretical approach for simulating photoinduced PCET with a surface hopping method[35,36] in conjunction with stochastic Langevin dynamics on electron-proton vibronic free energy surfaces that depend on a single collective solvent coordinate.[37] This approach is based on the multistate continuum theory of nonadiabatic PCET,[38] but the collective solvent coordinate is associated with the energy gap in a reduced two-state model of PCET.[39] The application of this approach to a series of model photoinduced PCET systems elucidated fundamental aspects of nonequilibrium PCET dynamics and clarified the origins of the observed isotope effects on the relaxation dynamics.[40] Since this approach is based on a reduced two-state model for PCET, however, it is capable of describing only concerted EPT processes. Moreover, the effects of proton vibrational relaxation were not included explicitly in this approach, so proton vibrational relaxation could occur only indirectly via nonadiabatic EPT transitions.

In the present paper, we develop a multidimensional generalization of our previous approach. This methodology is based on the multistate continuum theory with an arbitrary number of diabatic electronic states describing all relevant charge distributions in a general PCET system with multiple electron and proton donors and acceptors. The active electrons and transferring proton(s) are treated quantum mechanically, and the solvent dynamics is described by coupled Langevin equations for a set of collective scalar solvent coordinates. A surface hopping method is used to simulate the nonadiabatic dynamics on the multidimensional electron-proton vibronic free energy surfaces that depend on the collective solvent coordinates. This methodology allows the description of sequential as well as concerted mechanisms of photoinduced PCET. Moreover, this approach explicitly includes the effects of proton vibrational relaxation, intramolecular vibrational modes, and solvent dynamical effects. As an illustration, we analyze the results of simulations for two representative PCET model systems that differ by the arrangement of the ET and PT interfaces, corresponding to collinear and orthogonal PCET. These model systems are described in terms of a four-state model, resulting in two collective solvent coordinates corresponding to ET and PT, respectively. Analysis of the nonadiabatic dynamics on the two-dimensional electron-proton vibronic free energy surfaces provides insight into the roles of proton vibrational relaxation and nonequilibrium solvent dynamics. These simulations also illustrate concerted, sequential, and combined mechanisms for photoinduced PCET processes

The paper is organized as follows. In Sec. II, we present the theoretical formulation for the multidimensional treatment of photoexcited PCET reactions. This section describes the multistate model of the PCET reaction complex, the interaction of this complex with a continuum solvent environment, the calculation of the electron-proton vibronic free energy surfaces, the derivation of the coupled Langevin equations for the collective solvent coordinates, and the methodology for mixed quantum-classical nonadiabatic dynamics on the vibronic free energy surfaces. In Sec. III, we describe the model systems, the initial conditions, and the simulation details. Section IV presents our analysis of the simulations for the collinear and orthogonal PCET models with and without an energy bias for two different initial conditions. Concluding remarks are provided in Sec. V.

II. THEORY

A. Multistate model of the PCET reaction complex

Our model is based on a PCET reaction complex that consists of two coupled interfaces. The ET interface is comprised of the electron donor (D_e) and acceptor (A_e) groups connected by a molecular bridge. The PT interface is comprised of a hydrogen-bonded pair of proton donor (D_p) and acceptor (A_p) groups and the transferring proton. The spatial arrangement of the ET and PT interfaces and the nature of the donors, acceptors, and molecular bridge are general in this model and will be determined by the specific molecular system studied. The proton coordinate $\mathbf{r}_p$ and a set of specified intramolecular nuclear coordinates $\mathbf{Q}$ characterizing the configuration of the PCET reaction complex are treated explicitly in this model. Typically only a few intramolecular nuclear coordinates directly relevant to the PCET reaction will be retained. For example, the coordinate corresponding to the proton donor-acceptor distance is expected to be strongly coupled to the proton motion. In addition, torsional angles within the bridge connecting the ET donor and acceptor might be essential for describing the ET process, particularly for conjugated systems. In the following treatment, we assume the adiabatic separation between the "fast" degrees of freedom, which include the electron and proton coordinates, and the "slow" coordinates $\mathbf{Q}$.

A typical PCET reaction can be represented in terms of four diabatic electronic states, $|1a\rangle$, $|1b\rangle$, $|2a\rangle$, and $|2b\rangle$,

describing all possible charge transfer states in the coupled ET ($1 \rightarrow 2$) and PT ($a \rightarrow b$) processes. Schematically, these four diabatic states can be represented as the following valence bond states:[38]

$$\begin{aligned} &(1a)\ \mathrm{D_e^{\ominus}}\ \mathrm{D_p} - \mathrm{H} \cdots \mathrm{A_p^{\ominus}}\ \mathrm{A_e}, \\ &(1b)\ \mathrm{D_e^{\ominus}}\ \mathrm{D_p^{\ominus}} \cdots \mathrm{H} - \mathrm{A_p}\ \mathrm{A_e}, \\ &(2a)\ \mathrm{D_e}\ \mathrm{D_p} - \mathrm{H} \cdots \mathrm{A_p^{\ominus}}\ \mathrm{A_e^{\ominus}}, \\ &(2b)\ \mathrm{D_e}\ \mathrm{D_p^{\ominus}} \cdots \mathrm{H} - \mathrm{A_p}\ \mathrm{A_e^{\ominus}}. \end{aligned} \tag{1}$$

This minimal basis is designed to describe all possible mechanisms of the PCET process in which one electron and one proton transfer. Using the state $|1a\rangle$ as a reference (reactant) state, we can associate the sequential mechanisms with $1a \rightarrow 2a \rightarrow 2b$ (ET-PT) and $1a \rightarrow 1b \rightarrow 2b$ (PT-ET) and the concerted mechanism with $1a \rightarrow 2b$ (EPT). More complex cases, such as systems with multiple ET or PT interfaces, may require additional basis states. In such cases, the generalization to models with a larger number of diabatic states is straightforward.[38,41]

The gas phase electronic Hamiltonian in the basis of N diabatic electronic states is represented as

$$H_0^{\mathrm{el}}(\mathbf{r}_\mathrm{p}, \mathbf{Q}) = \sum_{i,j}^{N} h_{ij}(\mathbf{r}_\mathrm{p}, \mathbf{Q})\, |i\rangle\, \langle j|, \tag{2}$$

where $h_{ij}(\mathbf{r}_\mathrm{p}, \mathbf{Q})$ are the matrix elements of the gas phase electronic Hamiltonian in the diabatic basis. The diagonal elements $h_{ii}(\mathbf{r}_\mathrm{p}, \mathbf{Q})$ are the potential energy surfaces for the corresponding diabatic states, and the off-diagonal elements represent the electronic couplings between the diabatic states. For specific applications, these matrix elements can be obtained either from electronic structure calculations using an appropriate diabatization technique[42] or defined in the framework of a parameterization scheme based on the model PCET reaction system.

B. Interaction with continuum solvent environment: Vibronic free energy surfaces

In this model, the solvent is represented as an isotropic and uniform dielectric continuum described by a frequency-dependent complex-valued dielectric function $\varepsilon(\omega)$. In this case, the solvent orientational degrees of freedom are represented by the inertial polarization field $\mathbf{P}(\mathbf{r})$, which depends on the spatial coordinate $\mathbf{r}$. The procedure for separating the non-inertial (electronic) part of the polarization, $\mathbf{P}^{\infty}(\mathbf{r})$, from the total polarization, $\mathbf{P}^{\mathrm{tot}}(\mathbf{r}) = \mathbf{P}(\mathbf{r}) + \mathbf{P}^{\infty}(\mathbf{r})$, is well-established in the literature.[43–46] In the present treatment, we adopt the so-called Born-Oppenheimer limit, where the response of the solvent electrons is assumed to be infinitely fast compared to the active electrons of the PCET reaction complex.[44] In this limit, the interaction of the reaction complex with the polarization field of the solvent is introduced into the electronic Hamiltonian of the combined system in the following manner:

$$\begin{aligned} H^{\mathrm{el}}[\mathbf{r}_\mathrm{p}, \mathbf{Q}, \mathbf{P}(\mathbf{r})] = H_0^{\mathrm{el}}(\mathbf{r}_\mathrm{p}, \mathbf{Q}) + \sum_{i,j}^{N} \big(V_{ij}^{\mathrm{S}}\big[\mathbf{P}_{ij}^{\infty}(\mathbf{r})\big] \\ + V_{ij}^{\mathrm{S}}[\mathbf{P}(\mathbf{r})]\big)\, |i\rangle\, \langle j|\,. \end{aligned} \tag{3}$$

The interaction matrix elements $V_{ij}^{\mathrm{S}}[\mathbf{P}(\mathbf{r})]$ depend on $\rho_{ij}(\mathbf{r})$, the matrix elements of the total charge density operator for the reaction complex. These interaction matrix elements are given by the following volume integrals:

$$\begin{aligned} V_{ij}^{\mathrm{S}}[\mathbf{P}(\mathbf{r})] &= \iint dV\, dV'\, \frac{\rho_{ij}(\mathbf{r})\mathbf{P}(\mathbf{r}') \cdot (\mathbf{r} - \mathbf{r}')}{|\mathbf{r} - \mathbf{r}'|^3} \\ &= -\int dV\, \mathbf{P}(\mathbf{r}) \cdot \mathbf{D}_{ij}(\mathbf{r}), \end{aligned} \tag{4}$$

where $\mathbf{D}_{ij}(\mathbf{r})$ is the dielectric displacement field (i.e., vacuum electric field) induced by the charge density $\rho_{ij}(\mathbf{r})$. The matrix elements $V_{ij}^{\mathrm{S}}[\mathbf{P}^{\infty}(\mathbf{r})]$ represent the interaction of the charge density $\rho_{ij}(\mathbf{r})$ with the fully equilibrated, non-inertial part of the total polarization. These terms can be regarded as the electronic solvation terms for the reaction complex. In the remainder of the paper, we will omit these terms from all equations, assuming that they are implicitly included in the matrix elements of the gas phase Hamiltonian.

We invoke several approximations to simplify the derivations below. Note that the interaction matrix elements defined in Eq. (4) do not depend on the proton coordinate or on the other intramolecular coordinates $\mathbf{Q}$. This approximation is based on the assumption that the diabatic electronic states correspond to strongly localized charge densities with diabatic charge densities $\rho_{ij}(\mathbf{r})$ that depend only weakly on the intramolecular coordinates. Moreover, as the range of the proton motion ($\sim$0.5 Å) is small compared to the typical size of the reaction complex, the proton position does not significantly influence the total charge densities. Finally, we also assume that the off-diagonal densities, $\rho_{ij}(\mathbf{r})$, $i \neq j$, vanish because of the strongly localized character of the diabatic electronic states, so only the diagonal interaction matrix elements will be included in the summation of Eq. (3).

Within this formalism, the electron-proton vibronic Hamiltonian for the solvated reaction complex is defined as

$$H^{\mathrm{vib}} = T_\mathrm{p} + H^{\mathrm{el}}[\mathbf{r}_\mathrm{p}, \mathbf{Q}, \mathbf{P}(\mathbf{r})], \tag{5}$$

where the kinetic energy operator $T_\mathrm{p} = (-\hbar^2/2m_\mathrm{p})\nabla_\mathrm{p}^2$ for the proton with mass m_p. The eigenvalues of this electron-proton vibronic Hamiltonian, $W_n[\mathbf{Q}, \mathbf{P}(\mathbf{r})]$, can be obtained by the diagonalization of this Hamiltonian in an appropriate electron-proton vibronic basis. Following the procedure outlined in Ref. 41, the free energy functionals corresponding to the electron-proton vibronic states of the PCET reaction complex are given by the following general expression:

$$\mathcal{U}_n\,[\mathbf{Q}, \mathbf{P}(\mathbf{r})] = \frac{f_0}{2} \int |\mathbf{P}(\mathbf{r})|^2\, dV + W_n[\mathbf{Q}, \mathbf{P}(\mathbf{r})], \tag{6}$$

where $f_0 = 4\pi\varepsilon_0\varepsilon_\infty/(\varepsilon_0 - \varepsilon_\infty)$ is the inverse Pekar factor, and ε_0 and ε_∞ are the static (inertial) and optical (electronic) dielectric constants. The first term in Eq. (6), which is referred to as the self-energy term, depends quadratically on the inertial polarization field and represents the free energy of the solvent polarization field itself. This term incorporates the entropic contributions from the dielectric continuum solvent. The second term, which is referred to as the interaction term, accounts for the energy of the reaction complex and its interaction with the solvent polarization field. This term does

not include entropic contributions because the interaction between the reaction complex and the solvent polarization field is assumed to be purely electrostatic, neglecting the temperature dependence of the dielectric constants.

The interaction terms of the free energy functionals given in Eq. (6) can be recast in terms of $N-1$ scalar solvent coordinates $\{Y\}$ using the multistate continuum theory.[38] Omitting the technical details, the final expression for the free energy functionals corresponding to the electron-proton vibronic states of the solvated PCET reaction complex is

$$\mathcal{U}_n[\mathbf{Q},\mathbf{P}(\mathbf{r}),\{Y\}] = \frac{f_0}{2}\int |\mathbf{P}(\mathbf{r})|^2\,dV + \overline{W}_n(\mathbf{Q},\{Y\}) - \int \mathbf{P}(\mathbf{r})\cdot\mathbf{D}_{i_0 i_0}(\mathbf{r})\,dV, \tag{7}$$

where i_0 is the index of the diabatic state chosen as the reference. The scalar solvent coordinates $Y_i[\mathbf{P}(\mathbf{r})]$, which are functionals of the inertial polarization field $\mathbf{P}(\mathbf{r})$, correspond to the differences in interaction energies of the diabatic charge distributions with the inertial polarization field of the solvent:

$$Y_i[\mathbf{P}(\mathbf{r})] = -\int \left[\mathbf{D}_{ii}(\mathbf{r}) - \mathbf{D}_{i_0 i_0}(\mathbf{r})\right]\cdot\mathbf{P}(\mathbf{r})\,dV. \tag{8}$$

Note that the free energy functionals do not depend on Y_{i_0} but rather depend only on the other $N-1$ scalar solvent coordinates $\{Y\}$. The interaction terms $\overline{W}_n(\mathbf{Q},\{Y\})$ are now ordinary functions of the intramolecular coordinates $\mathbf{Q}$ and the $N-1$ scalar solvent coordinates $\{Y\}$. Specifically, they are the eigenvalues of the following transformed electron-proton vibronic Hamiltonian:

$$\overline{H}^{\mathrm{vib}} = T_{\mathrm{p}} + \overline{H}^{\mathrm{el}}(\mathbf{r}_{\mathrm{p}},\mathbf{Q},\{Y\}), \tag{9}$$

where

$$\overline{H}^{\mathrm{el}}(\mathbf{r}_{\mathrm{p}},\mathbf{Q},\{Y\}) = \sum_{i,j}^{N}\left[h_{ij}(\mathbf{r}_{\mathrm{p}},\mathbf{Q}) + \delta_{ij}(1-\delta_{ii_0})Y_i\right]|i\rangle\langle j|. \tag{10}$$

Note that the eigenvalues are obtained by diagonalizing the transformed electron-proton vibronic Hamiltonian in an appropriate electron-proton vibronic basis.

C. Generalized Langevin equation for solvent coordinates

The solvent dynamics in the dielectric continuum approximation is governed by the generalized Langevin equation describing the fluctuations of the inertial polarization field $\mathbf{P}(\mathbf{r})$ occurring on the adiabatic free energy surface $\mathcal{U}_n$.[19,22,47–49] This equation has the form

$$(\hat{f} - f_0)\mathbf{P}(\mathbf{r},t) = -\frac{\delta\mathcal{U}_n[\mathbf{Q},\mathbf{P}(\mathbf{r})]}{\delta\mathbf{P}} + \mathbf{F}(\mathbf{r},t), \tag{11}$$

where $\mathbf{F}(\mathbf{r},t)$ is the time-dependent random field describing thermal fluctuations of the polarization, and $\hat{f}$ is a causal integral operator defined via its action on an arbitrary time-dependent function $g(t)$:

$$\hat{f}\,g(t) = \int_{-\infty}^{t} f(t-\tau)g(\tau)\,d\tau. \tag{12}$$

The integral kernel $f(t)$ is related to the frequency-dependent factor $f(\omega) = 4\pi\varepsilon(\omega)\varepsilon_\infty/[\varepsilon(\omega)-\varepsilon_\infty]$ through the inverse Fourier transform

$$f(t) = \frac{1}{2\pi}\int_{-\infty}^{\infty} f(\omega)\mathrm{e}^{-i\omega t}\,d\omega. \tag{13}$$

The dynamical equation for the inertial polarization field, Eq. (11), can be rewritten in terms of only the scalar solvent coordinates $\{Y\}$.[41] The resulting set of coupled integro-differential equations has the following form:

$$(\hat{f} - f_0)Y_i = -f_0\sum_{j\neq i_0} T'_{ij}\frac{\partial\overline{W}_n(\mathbf{Q},\{Y\})}{\partial Y_j} - f_0\left(Y_i - T_{ii_0}\right) + F_i(t), \tag{14}$$

where

$$F_i(t) = \int \mathbf{F}(\mathbf{r},t)\cdot\left[\mathbf{D}_{i_0 i_0}(\mathbf{r}) - \mathbf{D}_{ii}(\mathbf{r})\right]\,dV \tag{15}$$

is the scalar time-dependent random force. In the above expression,

$$T_{ij} = \frac{1}{f_0}\int \mathbf{D}_{ii}(\mathbf{r})\cdot\mathbf{D}_{jj}(\mathbf{r})\,dV \tag{16}$$

and

$$T'_{ij} = \frac{1}{f_0}\int \left[\mathbf{D}_{ii}(\mathbf{r}) - \mathbf{D}_{i_0 i_0}(\mathbf{r})\right]\cdot\left[\mathbf{D}_{jj}(\mathbf{r}) - \mathbf{D}_{i_0 i_0}(\mathbf{r})\right]\,dV \tag{17}$$

are the matrix elements of the full $[N\times N]$ and truncated $[(N-1)\times(N-1)]$ reorganization energy matrices, respectively.[38,41]

The coupled generalized Langevin equations given in Eq. (14) possess two disadvantageous properties. First, they do not satisfy the fluctuation-dissipation theorem (FDT) in its standard formulation.[50] Second, the random forces are cross-correlated, leading to difficulties in the numerical implementation. The desired properties can be restored by transforming the set of solvent coordinates $\{Y\}$, represented by the vector $\mathbf{Y}$, to a scaled, rotated, and shifted set of solvent coordinates $\{Z\}$, represented by the vector $\mathbf{Z}$:

$$\mathbf{Z} = \mathbb{S}^{-1/2}\mathbb{C}^{\mathrm{T}}[\mathbf{Y} - \mathbf{\Theta}] \tag{18}$$

Here $\mathbb{C}$ is the orthogonal $[(N-1)\times(N-1)]$ matrix comprised of the eigenvectors of the truncated reorganization energy matrix $\mathbb{T}'$, $\mathbb{S}$ is the diagonal matrix with elements $2f_0\lambda_i$, where λ_i are the eigenvalues of the matrix $\mathbb{T}'$, and $\mathbf{\Theta}$ is the column vector with components T_{ii_0}, $i\neq i_0$. In the new coordinate system, $\{Z\}$, the Langevin equations of motion acquire the following simple form

$$(\hat{f} - f_0)Z_i = -\frac{\partial\overline{W}_n(\mathbf{Q},\mathbf{Z})}{\partial Z_i} - f_0 Z_i + \tilde{F}_i(t), \tag{19}$$

where the new random forces $\tilde{F}_i(t)$ satisfy the standard FDT. The corresponding Fourier-transformed time-correlation functions in the classical (high-temperature) limit have the following form:

$$\left[\left\langle \tilde{F}_i(t)\tilde{F}_j(t')\right\rangle\right]_\omega = \frac{2k_BT}{\omega}\frac{\mathrm{Im}[\kappa(\omega)]}{|\kappa(\omega)|^2}\,\delta_{ij}, \tag{20}$$

where $\kappa(\omega) = [f(\omega)]^{-1}$ is the generalized susceptibility of the solvent.

In the simplest case of the four-state model for PCET given in Eq. (1) with reference state $|i_0\rangle \equiv |1a\rangle$, only two of the three scalar solvent coordinates Y_{1b}, Y_{2a}, and Y_{2b} are linearly independent because the charge densities of the diabatic electronic states are constructed to satisfy the relation $\rho_{2b} = \rho_{1b} + \rho_{2a} - \rho_{1a}$.[38] Thus, the interaction term in Eq. (7) becomes a function of only two scalar solvent coordinates, $Y_p \equiv Y_{1b}$ and $Y_e \equiv Y_{2a}$, which are associated with PT and ET, respectively. In this case, $Y_{2b} = Y_p + Y_e$ and hence is not explicitly included in the dynamics. Analogously, we denote the two solvent coordinates Z_p and Z_e to be the transformed coordinates dominated by Y_p and Y_e, respectively.

For this simple case, the truncated reorganization energy matrix is a [2 × 2] matrix

$$\mathbb{T}' = \begin{pmatrix} 2\lambda_{PT} & 2\gamma \\ 2\gamma & 2\lambda_{ET} \end{pmatrix}, \tag{21}$$

where

$$\lambda_{PT} = \frac{1}{2}T'_{1b1b}, \quad \lambda_{ET} = \frac{1}{2}T'_{2a2a} \tag{22}$$

are the reorganization energies for PT and ET, respectively, and

$$\gamma = \frac{1}{2}T'_{1b2a} \tag{23}$$

is the cross-reorganization energy reflecting the strength of the electrostatic coupling of the PT and ET processes. The transformation matrices $\mathbb{C}$ and $\mathbb{S}$ have the following explicit forms:

$$\mathbb{C} = \begin{pmatrix} \cos\theta & -\sin\theta \\ \sin\theta & \cos\theta \end{pmatrix}, \quad \mathbb{S} = \begin{pmatrix} 2f_0\lambda_1 & 0 \\ 0 & 2f_0\lambda_2 \end{pmatrix}, \tag{24}$$

where the rotation angle θ is expressed as

$$\tan\theta = \frac{\lambda_{ET} - \lambda_{PT} - \sqrt{(\lambda_{ET} - \lambda_{PT})^2 + 4\gamma^2}}{2\gamma}, \tag{25}$$

and

$$\lambda_{1,2} = \frac{1}{2}(\lambda_{ET} + \lambda_{PT}) \mp \frac{1}{2}\sqrt{(\lambda_{ET} - \lambda_{PT})^2 + 4\gamma^2}. \tag{26}$$

The Langevin equations of motion given in Eq. (19) can be further simplified using the specific case of the Onodera model for dielectric relaxation of the solvent.[51] This model accounts for the inertial behavior of the polarization by introducing corrections to the conventional Debye model at short times (high frequencies). These corrections are associated with the characteristic rotational timescale of the solvent molecules. Following the formalism outlined in Ref. 37, the Langevin equations of motion assume the form

$$m_{\mathrm{eff}}\ddot{Z}_i = -f_0\tilde{\tau}_L\dot{Z}_i - \frac{\partial\overline{W}_n(\mathbf{Q},\mathbf{Z})}{\partial Z_i} - f_0 Z_i + \tilde{F}_i(t), \tag{27}$$

where the time correlation functions of the random forces are

$$\langle \tilde{F}_i(t)\tilde{F}_j(t')\rangle = 2\,k_BT\;f_0\;\tilde{\tau}_L\,\delta(t-t')\,\delta_{ij}, \tag{28}$$

and the other parameters are defined as

$$\tilde{\tau}_L = \frac{1}{\eta\,\omega_{\mathrm{rot}}^2\tau_D} + \frac{\varepsilon_\infty\tau_D}{\varepsilon_0}, \tag{29}$$

$$m_{\mathrm{eff}} = \frac{f_0}{\eta\omega_{\mathrm{rot}}^2}, \tag{30}$$

$$\eta = \frac{2\varepsilon_0 + \varepsilon_\infty}{3\varepsilon_0 g}, \quad \omega_{\mathrm{rot}}^2 = \frac{k_BT}{I}. \tag{31}$$

Here, τ_D is the Debye relaxation time of the solvent, g is the Kirkwood correlation factor, and ω_{rot} is the thermal rotational frequency, which depends on the moment of inertia I of the isolated solvent molecule. Following previous work, we assume that $\eta = 1$ in the present paper. Note that the friction, $f_0\,\tilde{\tau}_L$, is assumed to be a property of the solvent and thus to be the same for all vibronic states. Moreover, the effective solvent mass has units of (time)^2 because of the specific choice of solvent coordinates Z_p and Z_e, which have units of (energy)$^{1/2}$.

D. Mixed quantum-classical nonadiabatic dynamics on vibronic free energy surfaces

In photoinduced PCET processes, the relaxation dynamics involves nonadiabatic transitions between adiabatic vibronic free energy surfaces. Typically these transitions occur in regions where the energy splitting is small or at the seams of conical intersections. To incorporate nonadiabatic transitions into the dynamical treatment, we use Tully's fewest switches surface hopping algorithm, also denoted molecular dynamics with quantum transitions (MDQT).[35,36] In most implementations of this algorithm, an ensemble of trajectories is propagated on the adiabatic electronic potential energy surfaces. Each trajectory evolves classically on a single adiabatic surface but can instantaneously switch to another surface with a probability determined by the time-dependent amplitudes of the total electronic wavefunction. These quantum amplitudes are obtained by solving the time-dependent Schrödinger equation simultaneously with the propagation of the classical trajectories. The probabilistic algorithm used to incorporate the nonadiabatic transitions is designed to ensure that the fraction of trajectories in each state k at any time t is equal to the quantum probability determined from the quantum amplitudes. Details of the surface hopping algorithm[35,36] and our implementation for these types of processes[37] are given elsewhere.

In the present work, the solvent coordinates $\{Z\}$ evolve on the adiabatic electron-proton vibronic free energy surfaces according to the Langevin equations given in Eq. (27). The MDQT method can be applied to these free energy surfaces because only the solvent self-energy term includes entropic contributions, and the entropy is fixed during a nonadiabatic transition occurring at fixed values of the collective solvent coordinates. In addition, the intramolecular coordinates Q_k

with corresponding conjugate momenta P_k evolve according to the classical Hamilton equations of motion:

$$\dot{P}_k = -\frac{\partial H_n^{(Q)}}{\partial Q_k}, \quad \dot{Q}_k = \frac{\partial H_n^{(Q)}}{\partial P_k}, \tag{32}$$

where $H_n^{(Q)} = T_Q + \overline{W}_n(\mathbf{Q}, \mathbf{Z})$ is the classical Hamiltonian for motion of the intramolecular coordinates $\mathbf{Q}$ on the nth adiabatic vibronic state surface. In principle, the intramolecular coordinates could be treated with Langevin dynamics as well if they are coupled to the solvent.[52]

The quantitative accuracy of this approach may be limited by the approximations associated with a dielectric continuum representation of the solvent, linear response theory, and surface hopping. Nevertheless, this approach is expected to capture the qualitative aspects of photoinduced PCET processes. Comparison of the results to all-atom molecular dynamics simulations of explicit solute and solvent molecules described by an empirical valence bond potential, where the nonadiabatic dynamics is performed on electron-proton vibronic potential energy surfaces calculated on-the-fly, will assist in the assessment of the impact of some of these approximations. Methodological improvements, such as the inclusion of decoherence effects in the surface hopping algorithm and an additional solvent relaxation timescale, will also be explored in future work.

III. MODEL CALCULATIONS

A. Model systems

In this section, we illustrate the theoretical approach described in Sec. II using two simple five-site models representing typical PCET systems. The five sites correspond to the ET and PT donors and acceptors, as well as the transferring proton, which moves in one dimension along the PT donor-acceptor axis. No additional intramolecular coordinates within the reaction complex are included in these models. Two distinct geometries were chosen to represent PCET systems with strongly coupled and weakly coupled ET and PT. As depicted in Figure 1, the ET and PT interfaces are aligned along a common axis in Model I and are perpendicular to each other in Model II. We denote Models I and II as collinear PCET and orthogonal PCET, respectively. In both models, the ET and PT donor-acceptor distances are 7.0 Å and 2.5 Å, respectively.

The electronic subsystem is described in terms of the four diabatic states defined in Eq. (1). The gas phase potentials for the diabatic states are represented by the sum of a harmonic proton potential, $U_i^{\text{harm}}(r_p)$, an electrostatic Coulomb contribution, U_i^{Coul}, and an energy bias, Δ_i:

$$h_{ii}(r_p) = U_i^{\text{harm}}(r_p) + U_i^{\text{Coul}} + \Delta_i. \tag{33}$$

The proton potentials, $U_i^{\text{harm}}(r_p)$, are harmonic with a frequency of 3000 cm^{-1}, and the minimum is at $r_\text{p} = -0.25$ Å for the $1a$ and $2a$ states and at $r_\text{p} = 0.25$ Å for the $1b$ and $2b$ states, where the origin corresponds to the midpoint between the PT donor and acceptor. Note that the proton potentials are chosen to be harmonic to allow the relatively simple analytical evaluation of the matrix elements, but the calculations could be performed with any general proton potential. The energy at the minimum of the proton potential is determined by the electrostatic interaction energy, U_i^{Coul}, between the charges on the ET and PT donor and acceptor sites, as given in Table I. Since the charge on the transferring proton is chosen to be zero for all diabatic states, the interaction matrix elements defined in Eq. (4) are rigorously independent of the proton coordinate r_p. The charge on each donor and acceptor site is represented by a symmetric three-dimensional Gaussian distribution with exponent 0.1 Å^{-2}. The electrostatic energies of the $1b$, $2a$, and $2b$ diabatic states are calculated relative to the electrostatic energy of the $1a$ state. For Model I, the electrostatic energies are $U_{1a}^{\text{Coul}} = U_{2b}^{\text{Coul}} = 0$ and $U_{1b}^{\text{Coul}} = U_{2a}^{\text{Coul}} = 33.6$ kcal/mol. For model II, all four states have the same electrostatic energy of zero. For each model system, we studied two different cases of energy biases, Δ_i. In the first case, referred to as the symmetric models, the energy biases were zero for all four diabatic states. In the second case, which is indicated by a prime in the notation for the model systems, $\Delta_{1a} = \Delta_{1b} = 1$ eV, and $\Delta_{2a} = \Delta_{2b} = 0$. For all models, the coupling between the PT diabatic states is $h_{1a,\,1b} = h_{2a,\,2b} = 15$ kcal/mol, the coupling between the ET diabatic states is $h_{1a,\,2a} = h_{1b,\,2b} = 0.6918$ kcal/mol, and the second-order couplings are assumed to be zero (i.e., $h_{1a,\,2b} = h_{1b,\,2a} = 0$).

The solvent is chosen to be water, and all parameters corresponding to the solvent, such as τ_D, I, ε_0, and ε_∞, are given in Ref. 37. The reorganization energy matrix elements

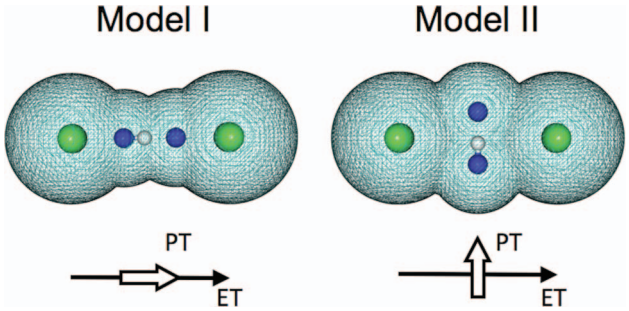

FIG. 1. Model systems for collinear PCET (Model I) and orthogonal PCET (Model II). The green balls denote the electron donor and acceptor sites, the blue balls denote the proton donor and acceptor sites, and the gray ball denotes the transferring hydrogen. The cavities constructed from overlapping spheres around the sites are also shown. These cavities are used for the FRCM calculations of the solvent reorganization energy matrix elements. The arrows below depict the direction of PT and ET in these model systems.

TABLE I. Radii and charges for the model PCET systems. ET and PT donor sites are denoted D_e and D_p, respectively; ET and PT acceptor sites are denoted A_e and A_p, respectively; and the transferring proton is denoted H. All of the quantities in this table are used to calculate the solvent reorganization energy matrix elements, and the charges are used to calculate the electrostatic contributions to the gas phase potentials of the reaction complex.

	D_e	D_p	H	A_p	A_e
Radii (Å)	3.5	2.7	1.2	2.7	3.5
$1a$ charges (e)	−1	0	0	−1	0
$1b$ charges (e)	−1	−1	0	0	0
$2a$ charges (e)	0	0	0	−1	−1
$2b$ charges (e)	0	−1	0	0	−1

TABLE II. Solvent reorganization energies, λ_{PT} and λ_{ET}, for PT and ET reactions, respectively, and cross-reorganization energy γ for the model PCET systems studied in this paper. Quantities given in units of kcal/mol.

	λ_{PT}	λ_{ET}	γ
Model I	4.35	19.27	−8.16
Model II	8.12	19.41	0

were calculated using the frequency-resolved cavity model (FRCM) (Ref. 53) with the point charges and radii for the sites given in Table I and the solvent parameters chosen to represent water. The reorganization energies, λ_{PT} and λ_{ET}, for the PT and ET reactions, respectively, as well as the cross-reorganization energy, γ, are given in Table II.

B. Initial conditions

The initial state in our calculations is chosen to be the direct product of the diabatic electronic state $|1a\rangle$ and the proton vibrational wavefunction $|\mu_0\rangle$ corresponding to the ground proton vibrational state of the electronic ground state that is occupied prior to photoexcitation. Note that the electronic ground state is not included in the dynamics following photoexcitation but rather is used only to determine the initial conditions in the excited states. At time $t = 0$, immediately after photoexcitation, the initial state is expanded in the basis of adiabatic vibronic states $|n\rangle$:

$$|\Psi(t=0)\rangle = |1a\rangle\,|\mu_0\rangle = \sum_n c_n^{(0)}|n\rangle, \quad c_n^{(0)} = \langle n|\,|1a\rangle|\mu_0\rangle. \tag{34}$$

The initial occupied state in each MDQT trajectory is determined with a probabilistic algorithm, where each adiabatic vibronic state $|n\rangle$ is sampled with a probability $|c_n^{(0)}|^2$. The adiabatic vibronic states $|n\rangle$ are linear combinations of the diabatic vibronic basis functions, and each diabatic vibronic basis function is the product of one of the four diabatic electronic states given in Eq. (1) and one of the associated proton vibrational states. Thus, the expansion coefficients $c_n^{(0)}$ depend on the Franck-Condon overlaps between the initial proton vibrational wavefunction $|\mu_0\rangle$ and the proton vibrational basis functions used in constructing the vibronic basis. According to this procedure, the initial population following photoexcitation is distributed among the adiabatic vibronic states dominated by the $1a$ diabatic electronic state.

Photoexcitation from the electronic ground state is assumed to be instantaneous for these calculations. We consider two different initial conditions, A and B, for each of the models, as illustrated in Figure 2. These initial conditions differ in the position of the proton potential of the electronic ground state relative to that of the photoexcited states, where the ground state proton potential is also harmonic with a frequency of 3000 cm^{-1}. Initial condition A corresponds to the situation where the minimum of the ground state proton potential is at the same position as the minimum of the proton potential in the photoexcited $1a$ state (i.e., at $r_p = -0.25$ Å). Initial condition B corresponds to the situation where the minimum of the ground state proton potential is midway between the minima of the proton potential in the photoexcited $1a$ and $1b$ states (i.e., at $r_p = 0$). Prior to photoexcitation, the system is assumed to be in the ground proton vibrational state of the electronic ground state. For initial condition A, the system is in the ground proton vibrational state of the $1a$ diabatic electronic state immediately following photoexcitation (i.e., at $t = 0$). For initial condition B, the system is in a coherent mixture of proton vibrational states corresponding to the $1a$ diabatic electronic state immediately following photoexcitation, where the amplitudes are determined by the Franck-Condon overlaps between the ground proton vibrational wavefunction of the electronic ground state and the proton vibrational wavefunctions associated with the $1a$ diabatic electronic state.

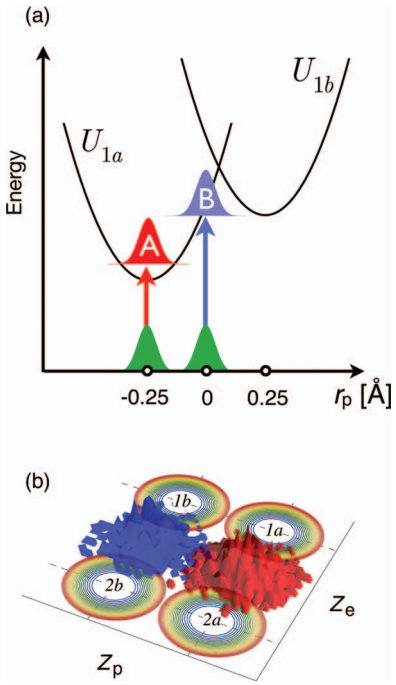

FIG. 2. Initial conditions used for the simulations. (a) Diabatic harmonic proton potentials, $U_i^{harm}(r_p)$, for the $1a$ and $1b$ diabatic electronic states and the initial proton wavepacket following photoexcitation (at $t = 0$) for the initial conditions A (red) and B (blue). The proton vibrational wavepacket prior to photoexcitation (green) corresponds to the ground proton vibrational state in the electronic ground state (not shown). (b) Initial distributions for the solvent coordinates Z_p and Z_e for the initial conditions A (red) and B (blue) for the symmetric Model II. The contour plot schematically depicts the four diabatic vibronic free energy surfaces with minima indicated as $1a$, $1b$, $2a$, and $2b$. For both initial conditions, the distributions are centered at $Z_e = 0$. The distributions are centered at the Z_p value corresponding to the $1a/2a$ minima for initial condition A and the $1b/2b$ minima for initial condition B.

The solvent configuration at time $t = 0$ is assumed to correspond to the classical Gaussian distribution associated with the potential of mean force $(1/2) f_0[(Z_p - Z_p^{(0)})^2 + (Z_e - Z_e^{(0)})^2]$ centered at values $(Z_p^{(0)}, Z_e^{(0)})$ discussed below. The resulting distribution has the form

$$\frac{f_0}{2\pi k_B T} \exp\left\{-\frac{f_0}{2k_B T}\left[\left(Z_p - Z_p^{(0)}\right)^2 + \left(Z_e - Z_e^{(0)}\right)^2\right]\right\}. \tag{35}$$

The initial values are chosen for the Y_p and Y_e coordinates, but the distributions are sampled according to the Z_p and Z_e

coordinates because the dynamics is propagated in terms of the Z_p and Z_e coordinates. Thus, our procedure is to determine the center of the distribution for the Y_p and Y_e coordinates, $Y_p^{(0)}$and $Y_e^{(0)}$, transform these values of the coordinates to $Z_p^{(0)}$and $Z_e^{(0)}$, and sample the initial Z_p and Z_e coordinates from Eq. (35). For both initial conditions A and B, the initial value of the ET solvent coordinate is determined according to the Gaussian distribution centered at $Y_e^{(0)} = 0$, which corresponds to the neutral molecule before photoexcitation. For initial condition A, the initial value of the PT solvent coordinate is determined according to the Gaussian distribution centered at the value of $Y_p = Y_p^{(1a)}$ corresponding to the equilibrium solvent configuration for the $1a$ diabatic state. This choice is consistent with the proton potential in the electronic ground state being similar to the proton potential in the $1a$ diabatic electronic state. For initial condition B, the initial value of the PT solvent coordinate is determined according to the Gaussian distribution centered at the value of $Y_p = Y_p^{(1b)}$ corresponding to the equilibrium solvent configuration for the $1b$ diabatic state. This choice is consistent with the electronic ground state proton potential being shifted relative to the proton potential in the $1a$ diabatic electronic state. For numerical reasons, however, this shift of the proton potential is only to the midpoint between the proton potentials in the $1a$ and $1b$ diabatic electronic states. The initial solvent coordinate distributions for Model II are depicted in Figure 2(b).

C. Simulation details

The adiabatic electron-proton vibronic free energy surfaces are obtained by diagonalization of the transformed vibronic Hamiltonian in Eq. (9) in an appropriate electron-proton vibronic basis. In this paper, the electron-proton vibronic basis functions are constructed as direct products of the diabatic electronic states and the proton vibrational states corresponding to the proton moving in the diabatic electronic potentials, $h_{ii}(r_p)$. We used 50 proton vibrational states for each diabatic electronic state, leading to a total of 200 electron-proton vibronic basis functions. The nonadiabatic coupling vectors required for propagating the surface hopping trajectories can be calculated analytically along the classical trajectories. The corresponding analytical expressions and other technical details of the calculations are described in our previous papers.[37,38]

For the MDQT trajectories, a time step of 0.1 fs is used to integrate the Langevin equation for the two classical solvent coordinates, and a variable time step that is 1/40 to 1/40,000 of the classical time step is used to integrate the time-dependent Schrödinger equation. In most cases, a quantum time step that is 1/40 the classical time step is sufficient to conserve the normalization of the time-dependent wavefunction during the quantum propagation. When the normalization of this wavefunction deviates from unity by more than 10^{-4}, however, the quantum propagation is repeated from the beginning of the classical time step with a quantum time step that is a factor of 10 smaller, and this procedure is continued until the normalization is conserved or the quantum time step is 1/40,000 of the classical time step.

In MDQT, the expectation value of an operator that is diagonal in the adiabatic basis can be calculated exactly because this procedure requires only the populations of the adiabatic states and not the coherences. Expectation values of operators that are not diagonal in the adiabatic basis, such as the diabatic state populations, depend on the coherences and thus are problematic within the MDQT formalism.[54] For this reason, we assign each adiabatic state to a diabatic state at each time step. Our assignment procedure involves calculating the expectation values of the projectors $\hat{P}_i = |i\rangle\langle i|$ on the diabatic electronic states $i = 1a$, $1b$, $2a$, and $2b$ for the occupied adiabatic electron-proton vibronic state, summing over the proton vibrational basis states, and assigning the occupied adiabatic state to the diabatic electronic state associated with the highest expectation value of the projector $\hat{P}_i$. In general, these four projection operators are not diagonal in the adiabatic basis. However, the off-diagonal elements are relatively small (i.e., typically the adiabatic state is dominated by a single diabatic electronic state), so this assignment procedure still provides physically reasonable results. The projectors $\hat{P}_1 = \hat{P}_{1a} + \hat{P}_{1b}$ and $\hat{P}_2 = \hat{P}_{2a} + \hat{P}_{2b}$ corresponding to the two different ET states are almost exactly diagonal in the adiabatic basis, except when the solvent coordinates are in close proximity to an avoided crossing, so the assignment to ET states 1 or 2 is very reliable.

IV. RESULTS

In this section, we analyze the results of simulations of mixed quantum-classical nonadiabatic dynamics for model photoinduced PCET systems. The key quantities characterizing the nonequilibrium photoinduced process are the populations of the adiabatic vibronic states, $P_n^{(ad)}$, the populations of the diabatic electronic states, $P_i^{(dia)}$ ($i = 1a$, $1b$, $2a$, $2b$), the distributions of the solvent coordinates in each of the adiabatic vibronic states, $P_n^{(solv)}(Y_p, Y_e)$, and the marginal solvent coordinate distributions, $P^{(solv)}(Y_p)$ and $P^{(solv)}(Y_e)$, for each of the solvent coordinates. The time-dependent populations of the adiabatic vibronic states are calculated by averaging the occupied adiabatic vibronic state at each time step over an ensemble of 1000 independent MDQT trajectories. The time-dependent populations of the diabatic electronic states are calculated by evaluating the expectation values of the projectors $\hat{P}_i = |i\rangle\langle i|$ for the occupied adiabatic vibronic state, assigning the occupied adiabatic vibronic state to a diabatic electronic state as described in Sec. III C, and averaging over the ensemble of MDQT trajectories. The time-dependent solvent coordinate distributions, $P_n^{(solv)}$, are calculated at each time step using a standard binning procedure for the solvent coordinates and assignment to the occupied adiabatic vibronic state for the ensemble of MDQT trajectories. The marginal solvent coordinate distributions are obtained by integrating the solvent coordinate distributions $P_n^{(solv)}$ over one of the solvent coordinates and summing over all adiabatic vibronic states:

$$P^{(solv)}(Y_p) = \sum_n \int P_n^{(solv)}(Y_p, Y_e)\, dY_e$$
$$P^{(solv)}(Y_e) = \sum_n \int P_n^{(solv)}(Y_p, Y_e)\, dY_p. \quad (36)$$

In our formulation, the dynamics of the photoinduced PCET process is represented as the time evolution of the solvent coordinate distributions $P_n^{(\mathrm{solv})}(Z_\mathrm{p}, Z_\mathrm{e})$ on the two-dimensional vibronic free energy surfaces

$$\mathcal{U}_n(Z_\mathrm{p}, Z_\mathrm{e}) = \frac{1}{2} f_0 \left(Z_\mathrm{p}^2 + Z_\mathrm{e}^2\right) + \overline{W}_n(Z_\mathrm{p}, Z_\mathrm{e}). \quad (37)$$

We present the time evolution of the solvent coordinate distributions as functions of the Z_p and Z_e coordinates because the dynamics is propagated in terms of these transformed solvent coordinates using the Langevin equations given in Eq. (27). In contrast, we present the time-dependent marginal solvent coordinate distributions as functions of the Y_p and Y_e coordinates because these solvent coordinates are associated directly with transitions between the diabatic electronic states via the definitions given in Eq. (8). Based on these definitions, motion along the Y_p solvent coordinate corresponds to the PT process, motion along the Y_e solvent coordinate corresponds to the ET process, and motion along the diagonal in the two-dimensional solvent coordinate space corresponds to the concerted EPT process. This interpretation is only qualitative because of the complicated coupling between these two solvent coordinates, which describe the time evolution of the polarization field of the dielectric continuum solvent.

Typically the two transformed solvent coordinates Z_p and Z_e are dominated by Y_p and Y_e, respectively, and therefore can also be associated with the PT and ET processes, respectively. For example, in Model II, the transformed solvent coordinates Z_p and Z_e are equivalent to the scaled and shifted, but not rotated, Y_p and Y_e coordinates due to the absence of coupling between the ET and PT processes (i.e., $\gamma = 0$). In some models, such as Model I, strong coupling between the ET and PT processes leads to substantial coupling between the two solvent coordinates, and the physical interpretation of the transformed solvent coordinates becomes more complicated. For this reason, the marginal solvent coordinate distributions are presented in terms of the original solvent coordinates Y_p and Y_e, even though the dynamics is propagated in terms of the transformed solvent coordinates Z_p and Z_e.

Additional information about the mechanism and the complex interplay between the PT and ET reactions can be inferred from the time evolution of the populations of the diabatic electronic states. Despite the approximate nature of the diabatic electronic state populations, as discussed in Sec. III C, our analysis indicates that the time evolution of these populations is consistent with the time evolution of the marginal solvent coordinate distributions. The remainder of this section presents analyses of model systems that illustrate fundamental aspects of photoinduced PCET.

A. Collinear PCET

The collinear PCET model, denoted Model I, represents a typical PCET system with strong electrostatic coupling between the ET and PT interfaces. As a result, the truncated reorganization energy matrix has a relatively large off-diagonal element, where the cross-reorganization energy is $\gamma = -8.16$ kcal/mol. The key dynamical quantities for the symmetric collinear PCET model (i.e., in the absence of an applied energy bias) with the initial conditions A and B are depicted in Figures 3 and 4, respectively. Due to the strong electrostatic interaction between the ET and PT interfaces, the diabatic electronic states $1a$ and $2b$ are significantly lower in energy than the diabatic electronic states $1b$ and $2a$ for the symmetric collinear PCET model. Specifically, this energy difference arises from the electrostatic attraction between the electron and proton when they are both on their donors or both on their acceptors. For simplicity, we denote the minima on the ground adiabatic vibronic surface in parts (c) of each figure by the dominant diabatic electronic state. For the symmetric collinear PCET model, the ground adiabatic vibronic surface has two minima dominated by the $1a$ and the $2b$ diabatic state, respectively. At thermal equilibrium, these two states have equal populations, and the solvent distribution is equally partitioned between these two minima.

For the initial condition A of Model I (Figure 3), most of the population at time $t = 0$ is in the first excited adiabatic vibronic state, and the solvent distribution is slightly displaced along Y_e from the $1a$ minimum of the ground adiabatic surface. Within the first picosecond, the system relaxes to the region near the $1a$ minimum on the ground adiabatic surface, undergoing nonadiabatic transitions along the seam of the avoided crossing between the ground and first excited states. The time-dependent marginal distributions for the solvent coordinates Y_p and Y_e depicted in Figure 3(b) illustrate that the solvent relaxation during this period occurs predominantly along the Y_e coordinate, while the Y_p coordinate fluctuates around its equilibrium value corresponding to the $1a$ diabatic state. During the following 4 ps, the system remains in the region of the $1a$ minimum on the ground adiabatic surface, and no PCET reaction is observed on this time scale. On a longer timescale, after equilibrium is reached, the populations of the $1a$ and $2b$ states will become equal. This behavior is very similar to the symmetric PCET model IA studied in our previous work,[37] which utilized a one-dimensional treatment of solvent dynamics within the framework of a two-state model.

For the initial condition B of Model I (Figure 4), the initial population is distributed among the higher excited vibronic states, reflecting the coherent mixture of proton vibrational states arising from the initially displaced proton vibrational wavepacket. The initial solvent distribution is displaced much further away from the minima of the ground adiabatic vibronic surface along both collective solvent coordinates. During the initial 0.5 ps, the system undergoes nonadiabatic transitions that result in concerted EPT ($1a$ to $2b$) in the highly excited vibronic states, leading to a fast displacement of the solvent distributions on the excited adiabatic vibronic surfaces toward the location of the $2b$ minimum. This behavior is clearly illustrated in Figures 4(a) and 4(b). Subsequently, the system undergoes multiple nonadiabatic transitions associated with proton vibrational relaxation, leading to the slowly growing population in the region near the $2b$ minimum on the ground adiabatic vibronic free energy surface, as illustrated in Figure 4(c). Qualitatively, the mechanism can be characterized as an initial fast concerted EPT in the highly excited vibronic states, followed by slower proton vibrational relaxation. As for the initial condition A, this

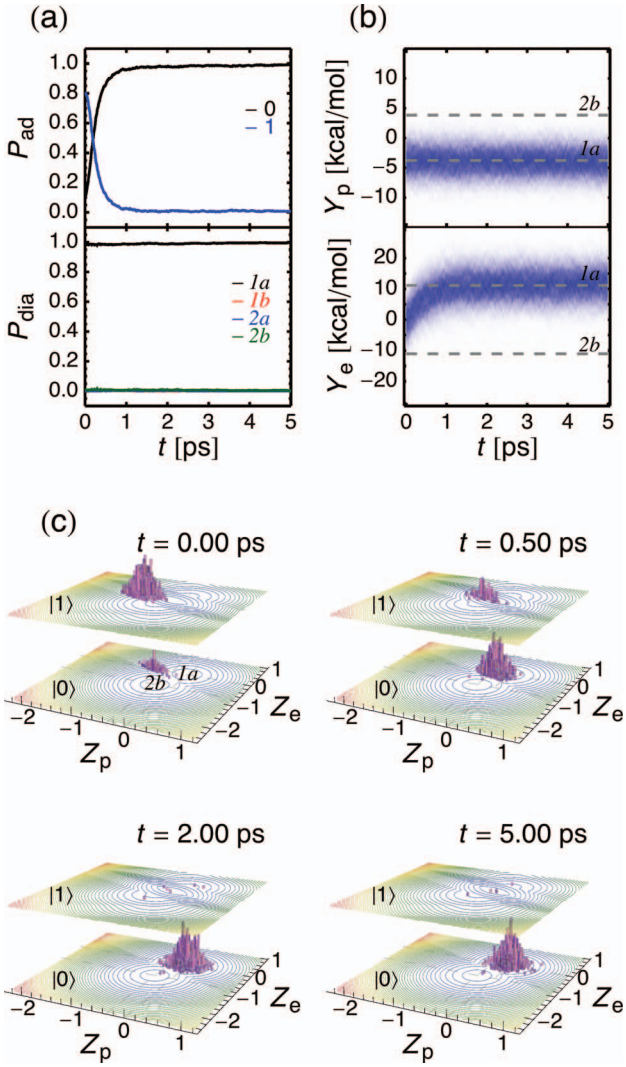

FIG. 3. Results for Model IA, the symmetric collinear PCET model system with initial condition A. (a) The time-dependent populations of the lowest two adiabatic vibronic states, $P_n^{(ad)}$, and the diabatic electronic states, $P_i^{(dia)}$ ($i = 1a, 1b, 2a, 2b$), where the notation for these populations is slightly altered for convenience. (b) The time-dependent marginal distributions, $P^{(solv)}(Y_p)$ and $P^{(solv)}(Y_e)$, for the collective solvent coordinates Y_p and Y_e, corresponding predominantly to PT and ET, respectively. The darker blue corresponds to a greater value of the marginal distribution function. The values of the solvent coordinates corresponding to the $1a$ and $2b$ minima on the diabatic vibronic surfaces are indicated by dashed lines. (c) Snapshots of the distributions, $P_n^{(solv)}(Z_p, Z_e)$, of the transformed solvent coordinates Z_p and Z_e in the lowest two adiabatic vibronic states along the trajectories. In the first snapshot, the minima of the ground adiabatic vibronic surface are labeled according to the dominant diabatic electronic state. See supplementary material for a movie of the time-dependent solvent distribution (Ref. 55).

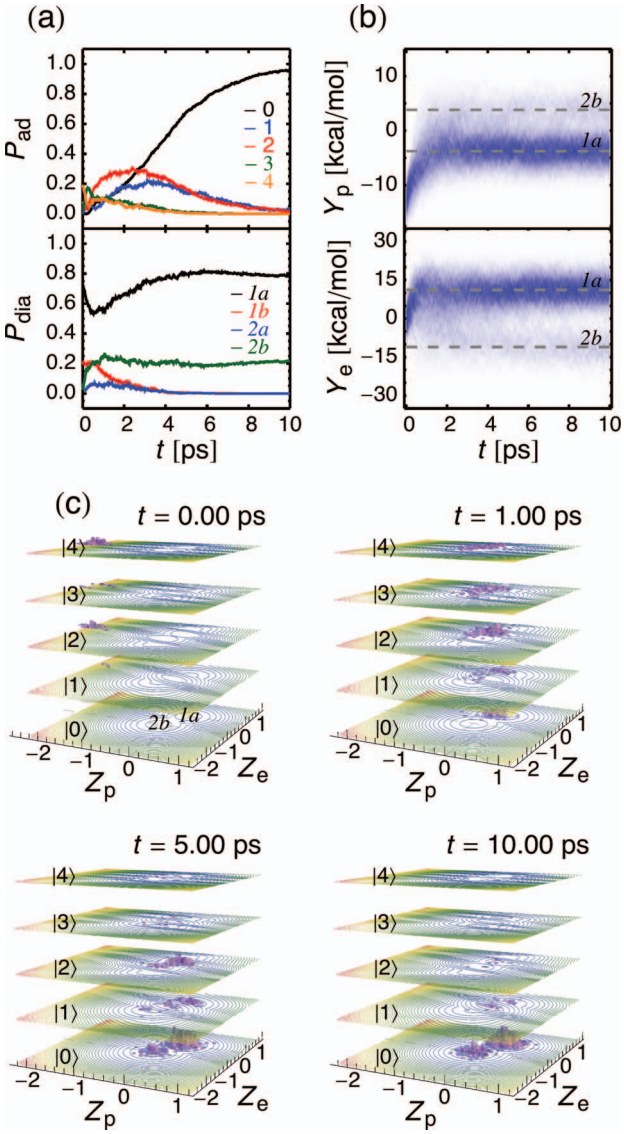

FIG. 4. Results for Model IB, the symmetric collinear PCET model system with initial condition B. (a) The time-dependent populations of the lowest five adiabatic vibronic states, $P_n^{(ad)}$, and the diabatic electronic states, $P_i^{(dia)}$ ($i = 1a, 1b, 2a, 2b$). (b) The time-dependent marginal distributions, $P^{(solv)}(Y_p)$ and $P^{(solv)}(Y_e)$, for the collective solvent coordinates Y_p and Y_e, corresponding predominantly to PT and ET, respectively. The darker blue corresponds to a greater value of the marginal distribution function. The values of the solvent coordinates corresponding to the $1a$ and $2b$ minima on the diabatic vibronic surfaces are indicated by dashed lines. (c) Snapshots of the distributions, $P_n^{(solv)}(Z_p, Z_e)$, of the transformed solvent coordinates Z_p and Z_e in the lowest five adiabatic vibronic states along the trajectories. In the first snapshot, the minimum of the ground adiabatic vibronic surface is labeled according to the dominant diabatic electronic state. See supplementary material for a movie of the time-dependent solvent distribution (Ref. 55).

mechanism is qualitatively similar to the previously studied symmetric PCET model (model IIA in Ref. 37). In the present two-dimensional treatment of the solvent dynamics, however, the relaxation occurs on a much shorter timescale (~10 ps) due to nonadiabatic transitions induced by the motion along the additional Z_p coordinate. As for model IA, the populations of the $1a$ and $2b$ states will eventually become equal after equilibrium is reached on a longer timescale.

These results are similar to those obtained in the framework of the two-state PCET model[37,40] because the diabatic electronic states $1b$ and $2a$ are much higher in energy than the diabatic electronic states $1a$ and $2b$ due to the attractive electron-proton Coulomb interactions. As a result, the four-state model for symmetric collinear PCET essentially reduces to the effective two-state ($1a$ and $2b$) model, and the solvent dynamics can be described in terms of a single collective solvent coordinate that is a linear combination of the two coordinates of the four-state model.

In the collinear PCET model with electronic bias (Model I′), the ground adiabatic vibronic surface has a

single minimum dominated by the 2*b* diabatic electronic state. The results for the initial condition A of Model I′ are depicted in Figure 5. The initial population mainly occupies the excited adiabatic vibronic states 5-7. During the first 3 ps following photoexcitation, a combination of ET (1*a* to 2*a*) and EPT (1*a* to 2*b*) processes is observed. Subsequently, the PT process corresponding to 2*a* to 2*b* transitions, as well as proton vibrational relaxation, is observed on a longer timescale (∼20 ps). After 20 ps, the system is primarily in the first excited adiabatic vibronic state in the region dominated by the 2*b* diabatic electronic state. Relaxation to the ground adiabatic vibronic state will occur on a much longer timescale due to the absence of significant nonadiabatic couplings in this region. Thus, this model illustrates a branching process, where one branch corresponds to a concerted EPT mechanism, and the other branch corresponds to a sequential ET-PT mechanism. These two distinct mechanisms are clearly illustrated in Figures 5(a) and 5(b). This behavior differs from the behavior observed for the models without an energy bias because the electron transfer states are energetically more accessible. The results for the initial condition B are qualitatively similar and are given in supplementary material (Fig. S1).[55]

B. Orthogonal PCET (Model II)

The idealized model of orthogonal PCET, denoted Model II, is characterized by the electrostatically uncoupled ET and PT interfaces with zero cross-reorganization energy. The main feature of the fully symmetric orthogonal PCET model is that the ground state vibronic free energy surface $\mathcal{U}_0(Z_p, Z_e)$ has four distinct degenerate minima dominated by the 1*a*, 1*b*, 2*a*, and 2*b* diabatic electronic states, respectively. At thermal equilibrium, all four of these states have equal populations, and the solvent distribution is equally partitioned among these four minima. The symmetric properties of the model allow us to study all possible combinations of the sequential and concerted pathways for the PCET process.

The results for Model II with the initial condition A are depicted in Figure 6. The initial population is distributed almost equally between the ground and first excited adiabatic vibronic states. At time $t = 0$, the solvent distribution is centered midway between the 1*a* and 2*a* minima of the ground adiabatic vibronic surface. This location corresponds to the region of strong nonadiabatic coupling along the seam of avoided crossing between the ground and first excited adiabatic vibronic surfaces. Consequently, within the first 200 fs, the system undergoes multiple nonadiabatic transitions of ET character (1*a* to 2*a*) and almost fully relaxes to the ground adiabatic vibronic state, nearly equally populating the regions near the 1*a* and 2*a* minima. This initial fast stage of dynamics is purely ET with no significant change in the populations of the 1*b* and 2*b* diabatic electronic states, as indicated by Figure 6(a). Moreover, Figure 6(b) indicates that the evolution of the solvent distribution occurs mainly along the Y_e coordinate during this time. Subsequently, the solvent distribution evolves on the ground adiabatic vibronic surface toward equilibrium by moving over the barriers along the Y_p coordinate, as illustrated by Figure 6(c). This model clearly exhibits a sequential ET-PT mechanism, with nonadiabatic ET followed by adiabatic PT on the ground adiabatic vibronic surface.

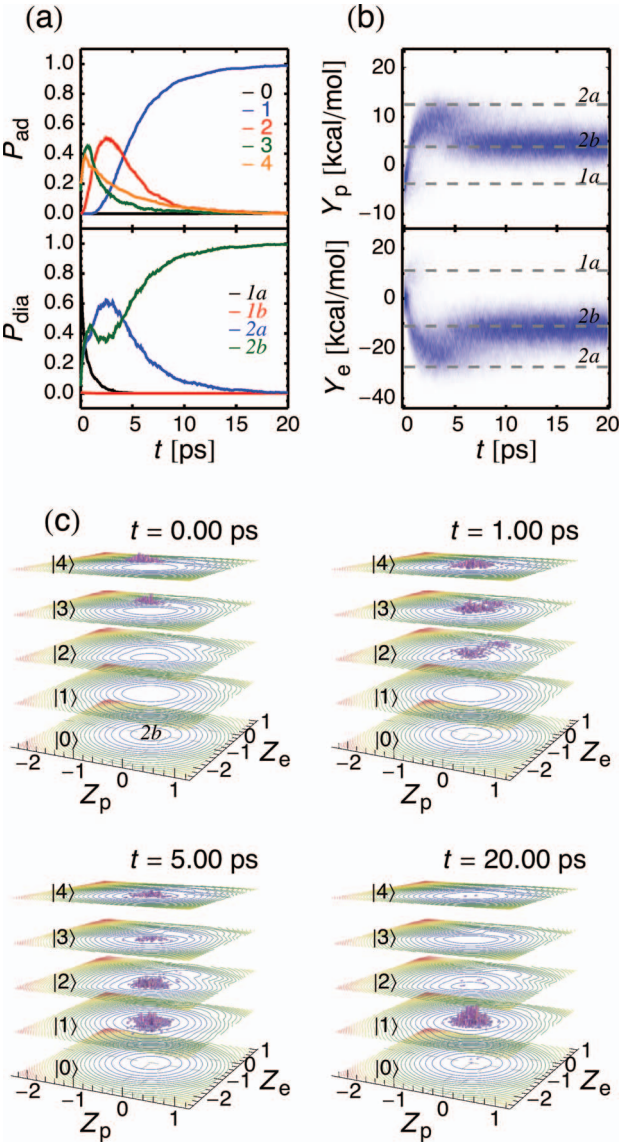

FIG. 5. Results for Model I′A, the biased collinear PCET model system with initial condition A. (a) The time-dependent populations of the lowest five adiabatic vibronic states, $P_n^{(ad)}$, and the diabatic electronic states, $P_i^{(dia)}$ ($i = 1a$, $1b$, $2a$, $2b$). (b) The time-dependent marginal distributions, $P^{(solv)}(Y_p)$ and $P^{(solv)}(Y_e)$, for the collective solvent coordinates Y_p and Y_e, corresponding predominantly to PT and ET, respectively. The darker blue corresponds to a greater value of the marginal distribution function. The values of the solvent coordinates corresponding to the 1*a*, 2*a,* and 2*b* minima on the diabatic vibronic surfaces are indicated by dashed lines. (c) Snapshots of the distributions, $P_n^{(solv)}(Z_p, Z_e)$, of the transformed solvent coordinates Z_p and Z_e in the lowest five adiabatic vibronic states along the trajectories. In the first snapshot, the minimum of the ground adiabatic vibronic surface is labeled according to the dominant diabatic electronic state. See supplementary material for a movie of the time-dependent solvent distribution (Ref. 55).

The results for Model II with initial condition B, corresponding to an initially displaced proton vibrational wavepacket, are depicted in Figure 7. In this case, the initial coherent mixture is dominated by higher excited adiabatic vibronic states. In the early stage of the dynamics (<1 ps), the solvent distribution quickly relaxes to the central region on the excited adiabatic vibronic surfaces. The excited state

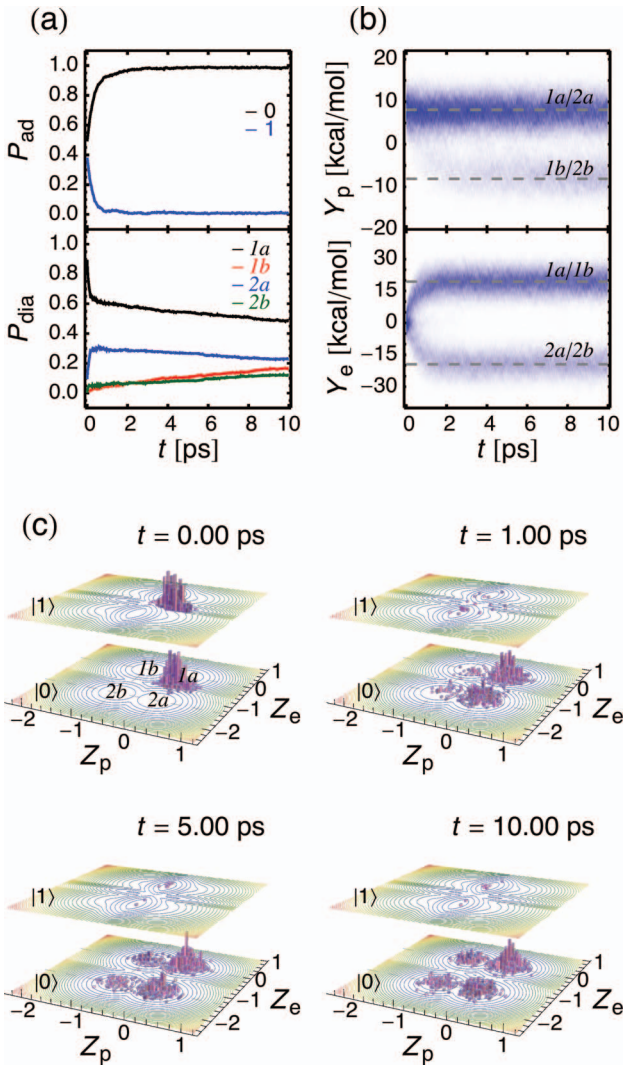

FIG. 6. Results for Model IIA, the symmetric orthogonal PCET model system with initial condition A. (a) The time-dependent populations of the lowest two adiabatic vibronic states, $P_n^{(ad)}$, and the diabatic electronic states, $P_i^{(dia)}$ ($i = 1a, 1b, 2a, 2b$). (b) The time-dependent marginal distributions, $P^{(solv)}(Y_p)$ and $P^{(solv)}(Y_e)$, for the collective solvent coordinates Y_p and Y_e, corresponding predominantly to PT and ET, respectively. The darker blue corresponds to a greater value of the marginal distribution function. The values of the solvent coordinates corresponding to the $1a$, $1b$, $2a$, and $2b$ minima on the diabatic vibronic surfaces are indicated by dashed lines. (c) Snapshots of the distributions, $P_n^{(solv)}(Z_p, Z_e)$, of the transformed solvent coordinates Z_p and Z_e in the lowest two adiabatic vibronic states along the trajectories. In the first snapshot, the minima of the ground adiabatic vibronic surface are labeled according to the dominant diabatic electronic state. See supplementary material for a movie of the time-dependent solvent distribution (Ref. 55).

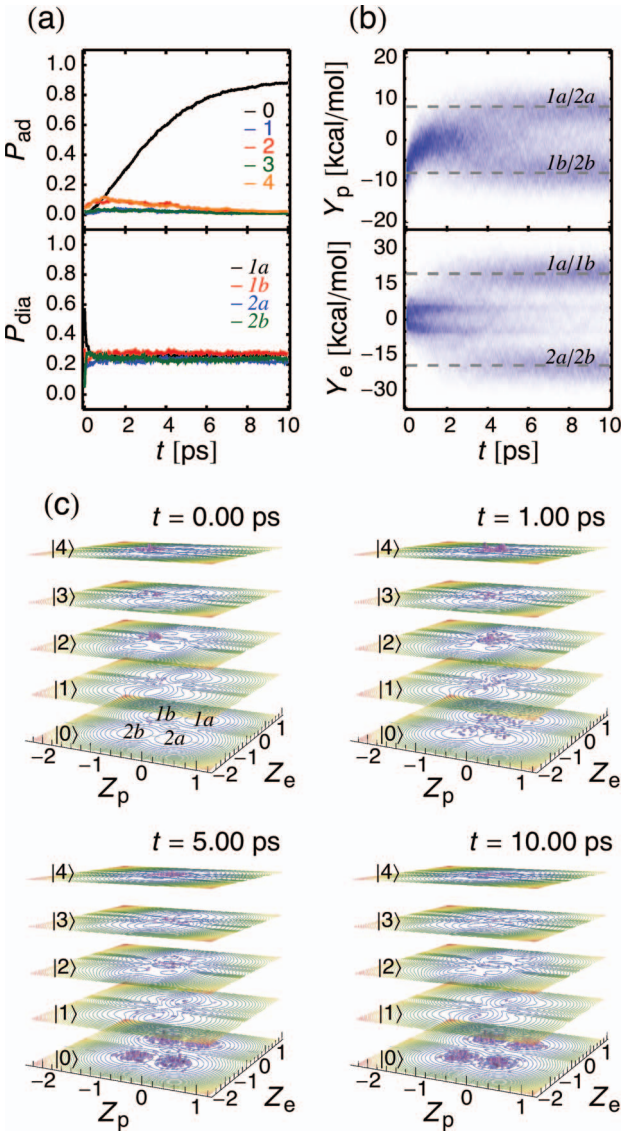

FIG. 7. Results for Model IIB, the symmetric orthogonal PCET model system with initial condition B. (a) The time-dependent populations of the lowest five adiabatic vibronic states, $P_n^{(ad)}$, and the diabatic electronic states, $P_i^{(dia)}$ ($i = 1a, 1b, 2a, 2b$). (b) The time-dependent marginal distributions, $P^{(solv)}(Y_p)$ and $P^{(solv)}(Y_e)$, for the collective solvent coordinates Y_p and Y_e, corresponding predominantly to PT and ET, respectively. The darker blue corresponds to a greater value of the marginal distribution function. The values of the solvent coordinates corresponding to the $1a$, $1b$, $2a$, and $2b$ minima on the diabatic vibronic surface are indicated by dashed lines. (c) Snapshots of the distributions, $P_n^{(solv)}(Z_p, Z_e)$, of the transformed solvent coordinates Z_p and Z_e in the lowest five adiabatic vibronic states along the trajectories. In the first snapshot, the minima of the diabatic vibronic surfaces are labeled according to the dominant diabatic electronic state. See supplementary material for a movie of the time-dependent solvent distribution (Ref. 55).

surfaces in this region are connected by strong nonadiabatic couplings forming a nearly vertical funnel, and the system follows this funnel down in energy, undergoing multiple nonadiabatic transitions. After ~10 ps, the system is almost entirely in the ground adiabatic vibronic state with the solvent distribution equally partitioned among the four minima. This PCET mechanism is difficult to classify due to its highly collective nature. Based on these analyses, an adequate description of the highly collective relaxation phenomena exhibited for the symmetric orthogonal PCET models requires the multidimensional treatment of the solvent dynamics in conjunction with nonadiabatic dynamics on the vibronic surfaces.

The figures illustrating the results for the orthogonal PCET model with electronic bias (Model II′) are provided in supplementary material (Figures S2 and S3).[55] Qualitatively, the relaxation mechanisms are similar to those observed for Model II, but the ground adiabatic vibronic surface has only two minima dominated by the $2a$ and $2b$ diabatic electronic states, respectively. For the initial condition A, the adiabatic

vibronic states 5-8 are populated following photoexcitation. In the first 200 fs after photoexcitation, a combination of ultrafast ET (1*a* to 2*a*) and EPT (1*a* to 2*b*) processes is observed, followed by slower ET and EPT processes of the same type. By 10 ps, the majority of the population (~60%) is in the ground vibronic state, evenly distributed between the regions near the 2*a* and 2*b* minima. For the initial condition B, the initial population is in the highly excited adiabatic vibronic states. Within ~2 ps, the solvent distribution moves to the central region, as in Model IIB. Subsequently, the solvent distribution follows the funnel down to populate the 2*a* and 2*b* minima on the ground adiabatic vibronic surface.

V. CONCLUDING REMARKS

In this paper, we developed a theoretical approach for the multidimensional treatment of photoinduced PCET processes in solution. In this formulation, the PCET process is described in terms of an arbitrary number of diabatic electronic states representing the relevant charge distributions in a general PCET system. The active electrons and transferring proton(s) are treated quantum mechanically, and the electron-proton vibronic free energy surfaces are represented as functions of multiple scalar solvent coordinates corresponding to the single electron and proton transfer reactions involved in the PCET process. In the simplest case, the PCET process is described in terms of two collective solvent coordinates corresponding to ET and PT, respectively. The solvent dynamics is described by a set of coupled Langevin equations of motion for these collective solvent coordinates. The parameters in the coupled Langevin equations are defined by the solvent properties, including the dielectric constants, Debye relaxation time, and molecular moment of inertia, as well as the solute properties characterizing the multidimensional electron-proton vibronic free energy surfaces. The dynamics of selected intramolecular nuclear coordinates, such as the proton donor-acceptor distance or a significant torsional angle within the PCET complex, may also be included in this formulation. A surface hopping method in conjunction with the Langevin equations of motion is used to simulate the nonadiabatic dynamics on the multidimensional electron-proton vibronic free energy surfaces following photoexcitation.

This theoretical treatment enables the description of both sequential (PT-ET and ET-PT) and concerted (EPT) mechanisms, as well as more complex processes involving a combination of sequential and concerted mechanisms. Our application of this methodology to a series of model systems corresponding to collinear and orthogonal PCET illustrated fundamental aspects of these different mechanisms. Furthermore, these applications elucidated the significance of proton vibrational relaxation, nonadiabatic transitions, and nonequilibrium solvent dynamics. In its current form, this approach does not include the fast librational motion associated with the first solvation shell around the PCET complex but rather includes only the slower solvent relaxation determined by the Debye relaxation time. Because the nonadiabatic transitions may occur during this faster solvent dynamics, inclusion of this faster solvent relaxation timescale may be important for these types of systems. Future work will focus on the extension of this theoretical approach to include two solvent relaxation timescales and the application of this approach to experimentally studied photoinduced PCET processes.[12,14]

ACKNOWLEDGMENTS

This material is based upon work supported by the Air Force Office of Scientific Research under AFOSR Award No. FA9550-10-1-0081 and NSF Grant CHE-07-49646. We thank Ben Auer for helpful discussions and comments on the manuscript.

[1] C. W. Hoganson, N. Lydakis-Simantiris, X.-S. Tang, C. Tommos, K. Warncke, G. T. Babcock, B. A. Diner, J. McCracken, and S. Styring, Photosynth. Res. **46**, 177 (1995).
[2] C. Tommos, X.-S. Tang, K. Warncke, C. W. Hoganson, S. Styring, J. McCracken, B. A. Diner, and G. T. Babcock, J. Am. Chem. Soc. **117**, 10325 (1995).
[3] M. Gratzel, Nature (London) **414**, 338 (2001).
[4] J. H. Alstrum-Acevedo, M. K. Brennaman, and T. J. Meyer, Inorg. Chem. **44**, 6802 (2005).
[5] E. M. Sproviero, J. A. Gascon, J. P. McEvoy, G. W. Brudvig, and V. S. Batista, Curr. Opin. Struct. Biol. **17**, 173 (2007).
[6] O. V. Prezhdo, W. R. Duncan, and V. V. Prezhdo, Acc. Chem. Res. **41**, 339 (2008).
[7] D. Gust, T. A. Moore, and A. L. Moore, Acc. Chem. Res. **42**, 1890 (2009).
[8] A. Magnuson, M. Anderlund, O. Johansson, P. Lindblad, R. Lomoth, T. Polivka, S. Ott, K. Stensjo, S. Styring, V. Sundstrom, and L. Hammarstrom, Acc. Chem. Res. **42**, 1899 (2009).
[9] K. de La Harpe, C. E. Crespo-Hernandez, and B. Kohler, J. Am. Chem. Soc. **131**, 17557 (2009).
[10] A. Kumar and M. D. Sevilla, Chem. Rev. **110**, 7002 (2010).
[11] B. Li, J. Zhao, K. Onda, K. D. Jordan, J. Yang, and H. Petek, Science **311**, 1436 (2006).
[12] C. J. Gagliardi, B. C. Westlake, C. A. Kent, J. J. Paul, J. M. Papanikolas, and T. J. Meyer, Coord. Chem. Rev. **254**, 2459 (2010).
[13] R. I. Cukier and D. G. Nocera, Annu. Rev. Phys. Chem. **49**, 337 (1998).
[14] J. J. Concepcion, M. K. Brennaman, J. R. Deyton, N. V. Lebedeva, M. D. E. Forbes, J. M. Papanikolas, and T. J. Meyer, J. Am. Chem. Soc. **129**, 6968 (2007).
[15] T. Irebo, S. Y. Reece, M. Sjodin, D. G. Nocera, and L. Hammarstrom, J. Am. Chem. Soc. **129**, 15462 (2007).
[16] B. C. Westlake, M. K. Brennaman, J. J. Concepcion, J. J. Paul, S. E. Bettis, S. D. Hampton, S. A. Miller, N. V. Lebedeva, M. D. E. Forbes, A. M. Moran, T. J. Meyer, and J. M. Papanikolas, Proc. Nat. Acad. Sci. U.S.A. **108**, 8554 (2011).
[17] S. Hammes-Schiffer, Proc. Nat. Acad. Sci. U.S.A. **108**, 8531 (2011).
[18] A. V. Barzykin, P. A. Frantsuzov, K. Seki, and M. Tachiya, Adv. Chem. Phys. **123**, 511 (2002).
[19] J. T. Hynes, J. Phys. Chem. **90**, 3701 (1986).
[20] I. Rips and J. Jortner, J. Chem. Phys. **87**, 2090 (1987).
[21] L. D. Zusman, Chem. Phys. **49**, 295 (1980).
[22] D. F. Calef and P. G. Wolynes, J. Phys. Chem. **87**, 3387 (1983).
[23] D. F. Calef and P. G. Wolynes, J. Chem. Phys. **78**, 470 (1983).
[24] A. Garg, J. Onuchic, and V. Ambegaokar, J. Chem. Phys. **83**, 4491 (1985).
[25] H. Sumi and R. Marcus, J. Chem. Phys. **84**, 4894 (1986).
[26] M. Sparpaglione and S. Mukamel, J. Chem. Phys. **88**, 3263 (1988).
[27] Y. J. Yan, M. Sparpaglione, and S. Mukamel, J. Phys. Chem. **92**, 4842 (1988).
[28] R. I. Cukier, J. Phys. Chem. **100**, 15428 (1996).
[29] A. V. Soudackov and S. Hammes-Schiffer, J. Chem. Phys. **113**, 2385 (2000).
[30] C. Venkataraman, A. V. Soudackov, and S. Hammes-Schiffer, J. Chem. Phys. **131**, 154502 (2009).
[31] J. Y. Fang and S. Hammes-Schiffer, J. Chem. Phys. **107**, 5727 (1997).
[32] J. Y. Fang and S. Hammes-Schiffer, J. Chem. Phys. **106**, 8442 (1997).

[33]C. Venkataraman, A. V. Soudackov, and S. Hammes-Schiffer, J. Chem. Phys. **131**, 154502 (2009).
[34]C. Venkataraman, A. V. Soudackov, and S. Hammes-Schiffer, J. Phys. Chem. C **114**, 487 (2010).
[35]J. C. Tully, J. Chem. Phys. **93**, 1061 (1990).
[36]S. Hammes-Schiffer and J. C. Tully, J. Chem. Phys. **101**, 4657 (1994).
[37]A. Hazra, A. V. Soudackov, and S. Hammes-Schiffer, J. Phys. Chem. B **114**, 12319 (2010).
[38]A. V. Soudackov and S. Hammes-Schiffer, J. Chem. Phys. **111**, 4672 (1999).
[39]S. Hammes-Schiffer and A. V. Soudackov, J. Phys. Chem. B **112**, 14108 (2008).
[40]A. Hazra, A. V. Soudackov, and S. Hammes-Schiffer, J. Phys. Chem. Lett. **2**, 36 (2011).
[41]M. V. Basilevsky, G. E. Chudinov, and M. D. Newton, Chem. Phys. **179**, 263 (1994).
[42]A. Sirjoosingh and S. Hammes-Schiffer, J. Phys. Chem. A **115**, 2367 (2011).
[43]M. V. Basilevsky and G. E. Chudinov, Chem. Phys. **165**, 213 (1992).
[44]J. N. Gehlen, D. Chandler, H. J. Kim, and J. T. Hynes, J. Phys. Chem. **96**, 1748 (1992).
[45]H. J. Kim and J. T. Hynes, J. Chem. Phys. **96**, 5088 (1992).
[46]H. J. Kim, R. Bianco, B. J. Gertner, and J. T. Hynes, J. Phys. Chem. **97**, 1723 (1993).
[47]B. U. Felderhof, J. Chem. Phys. **67**, 493 (1977).
[48]M. Y. Ovchinnikova, Khim. Fiz. **4**, 3 (1985).
[49]M. V. Basilevsky and G. E. Chudinov, Mol. Phys. **65**, 1121 (1988).
[50]L. D. Landau and E. M. Lifshitz, *Statistical Physics* (Pergamon, Oxford, 1980).
[51]Y. Onodera, J. Phys. Soc. Jpn. **62**, 4104 (1993).
[52]J. o. P. Malhado, R. Spezia, and J. T. Hynes, J. Phys. Chem. A **115**, 3720 (2011).
[53]M. V. Basilevsky, I. V. Rostov, and M. D. Newton, Chem. Phys. **232**, 189 (1998).
[54]U. Muller and G. Stock, J. Chem. Phys. **107**, 6230 (1997).
[55]See supplementary material at http://dx.doi.org/10.1063/1.3651083 for the analogous figures to Figures 3–7 for Models I′B, II′A, and II′B, and for movies of the time-dependent solvent distribution for all models.